Journal of
Materials Sciences and Applications

JScholar
Fostering Scholarly Communication

Research Article Open Access

Modeling of Texture Evolution of Aluminum Sheet under Ironing

Yihai S[1*] Wu PD[1], Jin H[2]

[1]Department of Mechanical Engineering, McMaster University, Canada
[2]Senior Research at Canmet, Canada

***Corresponding author:** Yihai S, Department of Mechanical Engineering, McMaster University, 1280 Main Street West, Hamilton, Ontario, Canada L8S 4L7. Tel: 647-888-8160, Email: shiyh@mcmaster.ca

Received Date: February 21, 2022 **Accepted Date:** March 23, 2022 **Published Date:** March 24, 2022

Citation: Yihai S, (2022) Modeling of Texture Evolution of Aluminum Sheet under Ironing. J Mater sci Appl 6: 1-16

Abstract

The finite element method is used to simulate the texture evolution in an aluminum sheet, AA6111, under ironing with a multi-level modeling approach. The measured electron backscatter diffraction (EBSD) data has been directly incorporated into the finite element sub-model and the constitutive response at an integration point is described by the single crystal plasticity theory. The effects of mesh sensitivity, coefficient of friction (COF), ironing pass and reduction on texture evolution in ironed sheet, are studied. It is found that grain refinement is mainly established in the first ironing pass. The friction-induced shear strain in each ironing pass also influences texture evolution/grain refinement even though such texture evolution may be path-independent as long as the total reduction keeps the same. It is also found that strain rate sensitivity and/or hardening may have limited influence grain refinement at the same ironing condition.

Keywords: Aluminum alloys; Ironing; Finite element analysis; EBSD; Crystal plasticity

Introduction

Draw and Iron (D&I) is a major sheet metal forming operation and extensively used in can manufacturing (including aluminum and steel can). Ironing is a process in which the wall thickness of a drawn cup is made uniform by the pushing of the cup through ironing dies[1]. The major goal of ironing process is to reduce the sheet gauge and achieve the desired length and thickness in a single operation. Ironing has been studied both experimentally and numerically. Early research [2] shows that ironing die geometry has a significant impact on sheet ironability. Heymis et al. [3] used a texture program popLA to perform metallographic studies on grain shape, local deformation modes and damage events of a strip aluminum alloy AA3004, which are of value in understanding the structural changes which arise in the ironing process. Abe et al. [4] investigated the friction influence on the ironing of stainless steel can with low friction cermet dies and found that low friction improves ironability in a continuous operation. High temperature ironing operation was studied by Singh et al. [5] both experimentally and numerically. The influence of ironing on the earring was studied by Anggono et al [6] for both aluminum alloy AA5042 and AKDQ steel.

Presently, most ironing researches focus on the operation of ironing (ironability) such as die geometry, friction and reduction etc. Less effort is placed on the material deformation behaviors during ironing. Ironing is a very unique metal forming process. When the sheet is forced passing through ironing dies, the material experiences severe shear and compressive strain. As pointed out by Heymis et al. [3], large shear strains presented in ironing and these can vary through the wall thickness. In simulation of ironing process, the model with inclusion of shear component gives rise of asymmetrical texture which agrees very well with observed experimentally. The shear texture is also commonly observed in other shear-induced deformation processes such as cold rolling [7-10] and equal-channel angular pressing (ECAP) or extrusion (ECAE) [11-14] and shearing is the major contributor to the grain refinement [13].

In this paper, the development of texture during strip ironing of the alloy AA6111 is studied through a crystal plasticity-based FEM, utilizing the grain orientations obtained from large-scale EBSD maps. Effects of strain work hardening, strain rate sensitivity, step size (mesh sensitivity), friction and ironing reduction on texture evolution and grain refinement will be discussed.

Experiment

The material used in the present work was a 0.93mm gauge commercial AA6111 T4 sheet, with nominal composition of Al-0.7Si-0.7Mg-0.7Cu-0.2Fe (wt.%). A coupon-sized specimen, 20 mm in the rolling direction (RD) and 4 mm in the transverse direction (TD), was cut from the sheet and mounted in conductive compound in the longitudinal section, which is defined by the RD and the normal direction (ND) as shown in Figure 1(a). The specimen was mechanically ground down to 1 μm diamond paste, mechanical-chemically polished by 0.05 μm colloidal silica in a Buehler Vibromet polisher for about 8 hours, followed by a light acidic etching in 0.5% HF water solution for about 20 seconds. The electron backscatter diffraction (EBSD) analysis was done in a Philips XL30 FEG scanning electron microscope (SEM) at 25 kV with a step size of 3 μm. The total scanned area was 5.907 mm in the RD and 0.903mm in the ND. To facilitate the strip ironing simulation, a sub-set area, 0.981mm in the RD and 0.903 mm in the ND, was randomly selected from the original large EBSD map, and it consists of a total of 99056 orientations (Figure 1(b)). The crystallographic texture of the sub-set is shown in Figure 1(c) in terms of the {1 1 1} pole figure. I t is actually very similar to the one generated from the entire EBSD map (not shown), so the sub-set represents the entire sheet well. The mean grain size determined by the EBSD is 20μm.

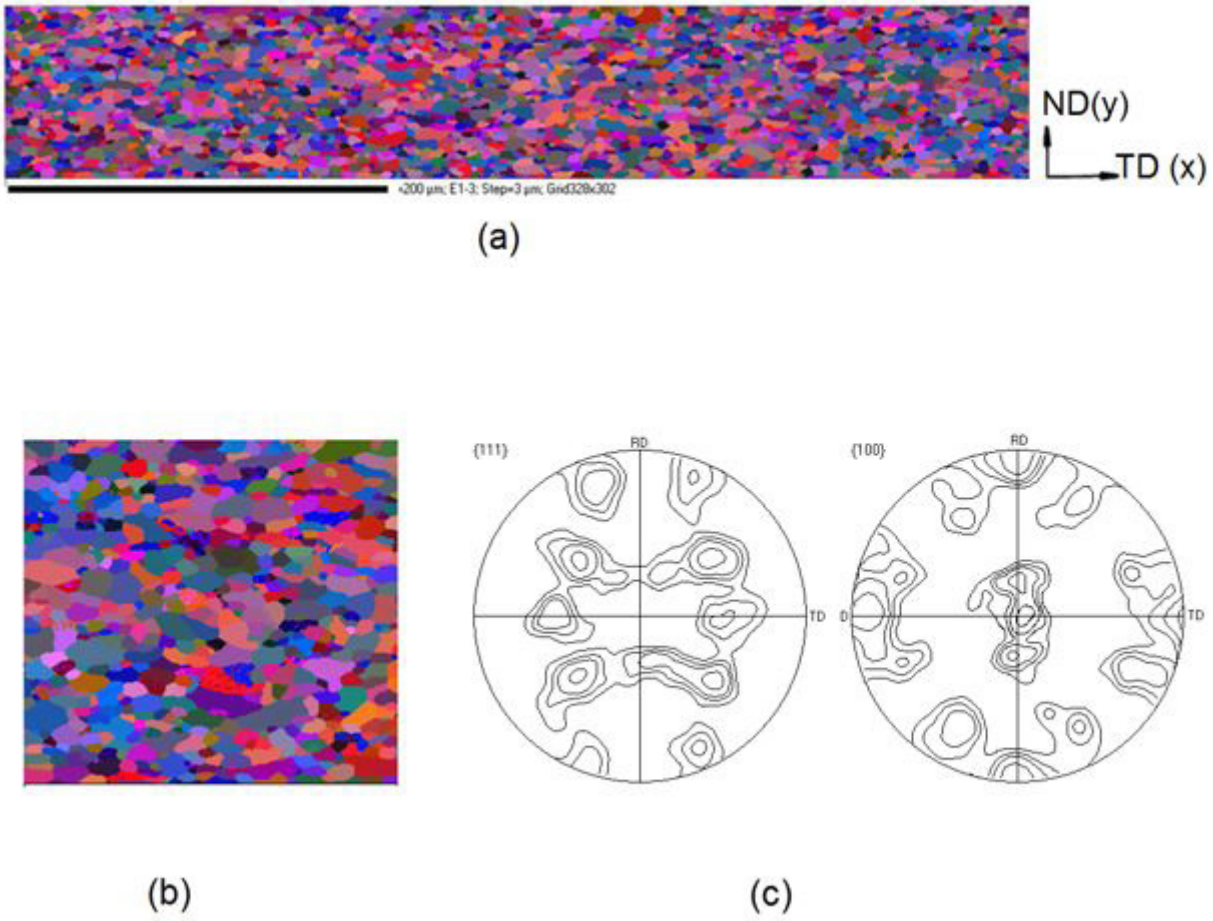

Figure 1: AA6111 sheet EBSD mapping, (a) AA6111 EBSD map; (b) selected sample for simulation, this selection area represents the sheet texture; (c) pole figure of the selected sample

Constitutive model and its calibration

A rate-dependent crystal plasticity described by Asaro and Needleman [15] and Wu et al. [16], is adopted to simulate the ironing process and will be briefly summarized in this section. The elastic constitutive equation of crystal plasticity model for each grain is specified by

$$\overset{\nabla}{\boldsymbol{\sigma}} = \mathbf{D} - \boldsymbol{\sigma}^{0} - \boldsymbol{\sigma}\,\mathrm{tr}\,\mathbf{D} \tag{1}$$

where $\overset{\nabla}{\boldsymbol{\sigma}}$ is the Jaumann rate of Cauchy stress, $\mathbf{L}$ represents the tensor of elastic moduli and $\mathbf{D}$ represents the strain-rate tensor. The term $\boldsymbol{\sigma}^{0}$ is a viscoplastic type stress rate that is determined by the slip rates on the various slip systems in the crystal. The slip rates are taken to be governed by the power-law expression:

$$\dot{\gamma}_{(\alpha)} = \dot{\gamma}_{(0)}\,\mathrm{sgn}\,\tau_{(\alpha)}\left|\frac{\tau_{(\alpha)}}{g_{(a)}}\right|^{1/m} \tag{2}$$

where $\dot{\gamma}_{(0)}$ is a reference shear rate taken to be the same for all the slip systems, $\tau_{(\alpha)}$ is the resolved shear stress on slip system α, $g_{(\alpha)}$ is the hardness and m is the strain-rate sensitivity index. The $g_{(\alpha)}$ characterizes the current strain hardened state of the crystal. For multiple slip systems, the evolution of the hardness is governed by

$$\dot{g}_{(\alpha)} = \sum_{\beta} h_{(\alpha\beta)}\left|\dot{\gamma}_{(\beta)}\right| \tag{3}$$

where $g_{(\alpha)}(0)$ is the initial hardness and is taken to be a constant τ_0 for each slip system, and $h_{(\alpha\beta)}$ values are the hardening moduli. The moduli are assumed to have the form

$$h_{(\alpha\beta)} = q_{(\alpha\beta)}h_{(\beta)} \tag{4}$$

where $h_{(\alpha\beta)}$ is a single slip hardening rate and $q_{(\alpha\beta)}$ is the matrix describing the latent hardening behaviour of the crystal (see e.g. Wu et al. [16]). The latter is determined by a latent

hardening parameter $q \geq 1$, if $q = 1$, then the hardening is isotropic. In this paper, the following slip hardening rate is used:

$$h_{(\beta)} = h_{(0)}\left(1 - \frac{g_{(\beta)}}{\tau_s}\right)^a \quad (5)$$

where $h_{(0)}$, a and τ_s are the slip system hardening parameters, taken to be identical for all slip systems. This constitutive model is implemented into a general finite element package ABAQUS [17] through a user materials subroutine UMAT.

The hardening parameters as specified in Equation 1 to Equation 5 are determined by curve-fitting. An iterative numerical approach was performed to simulate uni-axial tension in the RD with 500 grain orientations as inputs. The comparison of fitting curve and the corresponding experimental tensile data is plotted shown in Figure 2. Based on fitting, the material parameters in the crystal plasticity analysis are as follows: $C_{11} = 236$ GPa, $C_{12} = 135$ GPa and $C_{44} = 62$ GPa, $\dot{\gamma}_0 = 0.001\, s^{-1}$, $m = 0.007$, $\tau_0 = 48$ MPa, $h_0 / \tau_0 = 9.0$, $\tau_s / \tau_0 = 2.5$, $a = 1.3$ and $q = 1.4$. It is noted that the strain-rate sensitivity m and the slip system reference plastic shearing rate $\dot{\gamma}_0$ are in the typical range for rolled aluminum alloys.

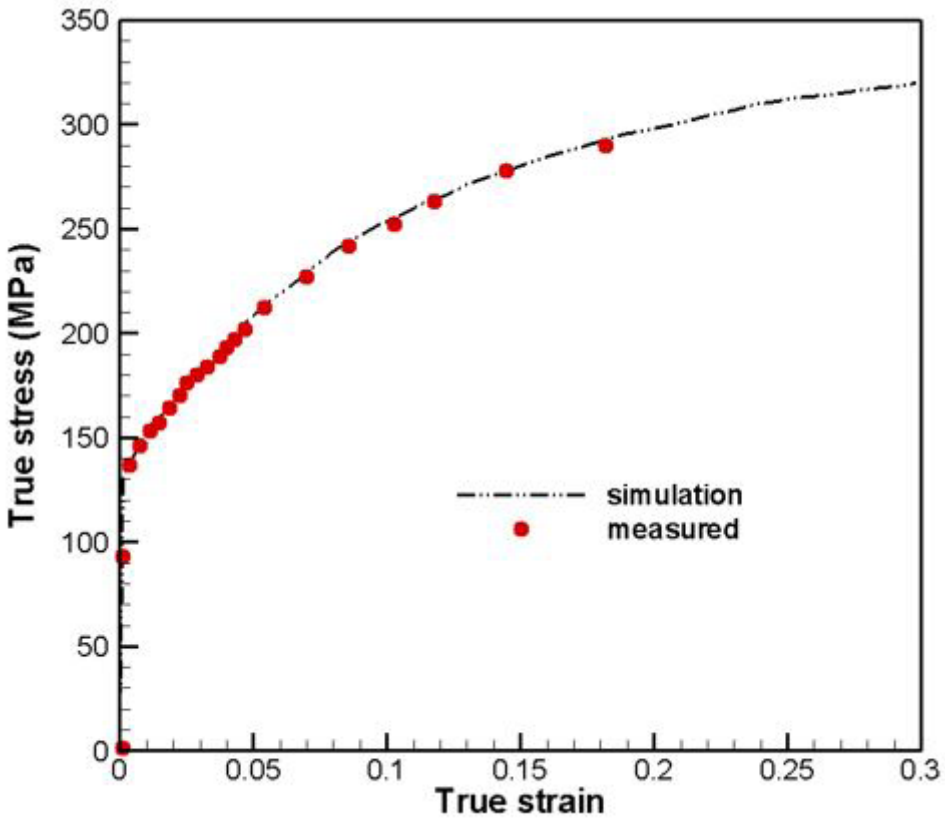

Figure 2: The measured and simulated tensile stress-strain curves along the rolling direction (RD)

Problem formulation and method of solution

Since the width of strip ironing is much longer than the thickness, the strip ironing process can be treated as plane strain deformation. A schematic ironing process is presented in Figure 3. The ironing sample is taken longitudinal section of sheet with initial thickness t_0. As shown in Figure 3 (b) and (c), the transverse direction (TD) of the sheet is aligned with x direction in ironing process and the normal (thickness) direction (ND) is aligned with y direction. Under the driving force of punch, this longitudinal section (TD-ND plane) of sheet passes through 3 ironing dies as shown in Figure 3(a). As the gap t between the punch outer surface and ironing die is less than the initial sheet thickness t_0, the sheet is forced to squeeze through the gap under shear and compression from the die, which results in the reduced

thickness t during each ironing pass. The success of ironing depends on many factors, such as material ironability and friction between the die and sheet. Form tooling point of view, the entry die angle α, the landing length *s*, and the exit die angle β in Figure

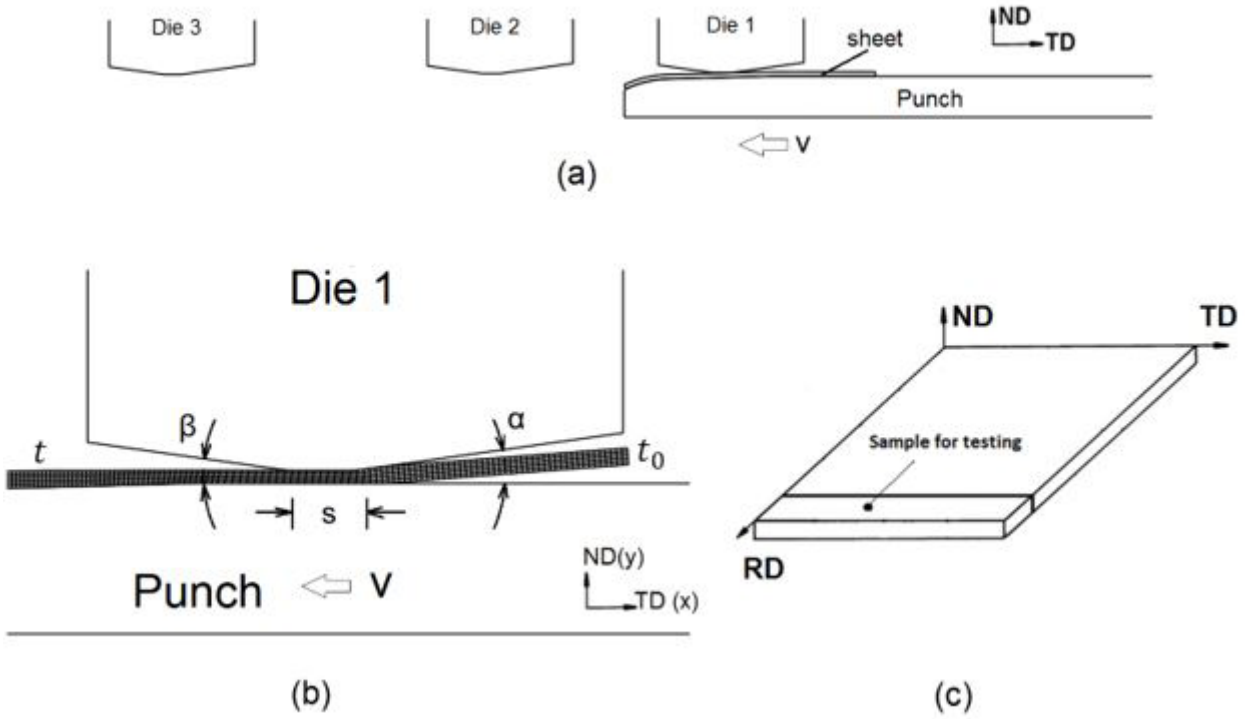

Figure 3: Schematics of strip ironing and its key dimensions, (a) longitudinal section of the sheet in strip ironing with three ironing dies; (b) key dimensions of ironing: α is die entry angle, β is die exit angle, s is landing lengh, t_0 is thickness before ironing, t is thickness after ironing and V is ironing velocity; (c) longitudinal section of the sheet

3(b) are the crucial elements.

The sample in the ironing process is in the scale of mm while the measured EBSD map in the crystal placidity model is in the scale of μm. To bridge this gap, a multi-level modeling technique is adopted to capture the sheet deformation behavior at the microstructure level but using ironing operating conditions at a macrostructure level. Meanwhile, a reasonable computational scheme has to be achieved in this multi-level modeling technique.

In Figure 4, two models, namely the global model and the sub-model, are used to simulate ironing process. Firstly, a sample sized plane strain 3-pass ironing is performed in the global model. All the ironing operating conditions are applied to the global model. Then a microstructurally based sub-model (also plane strain) is built at a selected region of the ironing sample for each pass and simulation is performed using EBSD microstructural data as inputs. The displacement history of the selected region is taken from the global model and applied as a boundary condition in the micro-model (sub-model). In the global model, the entire sheet specimen is meshed with linear rectangular plane strain elements with relative coarse meshing (4 elements through thickness). Subsequently, in the sub-model, a much finer mesh is chosen for the selected region, of which texture EBSD data can be mapped to the sub-model. In the sub-model of Figure 4, the selected region (area with 0.981 mm in length and 0.903 mm in height as described in Section 2) has 301 elements through thickness and 327 elements in length, representing exactly 3 m step size of the EBSD map. Three Euler angles of 99056 orientations from EBSD then mapped to the sub-model (99056 elements), one orientation per element. Four boundaries (a, b, c, d in Figure 4) in the selected region are driven by the displacement history of the sheet from the global model. ABAQUS provides a direct coupling in terms of displacement boundary conditions between the global model and the sub-model.

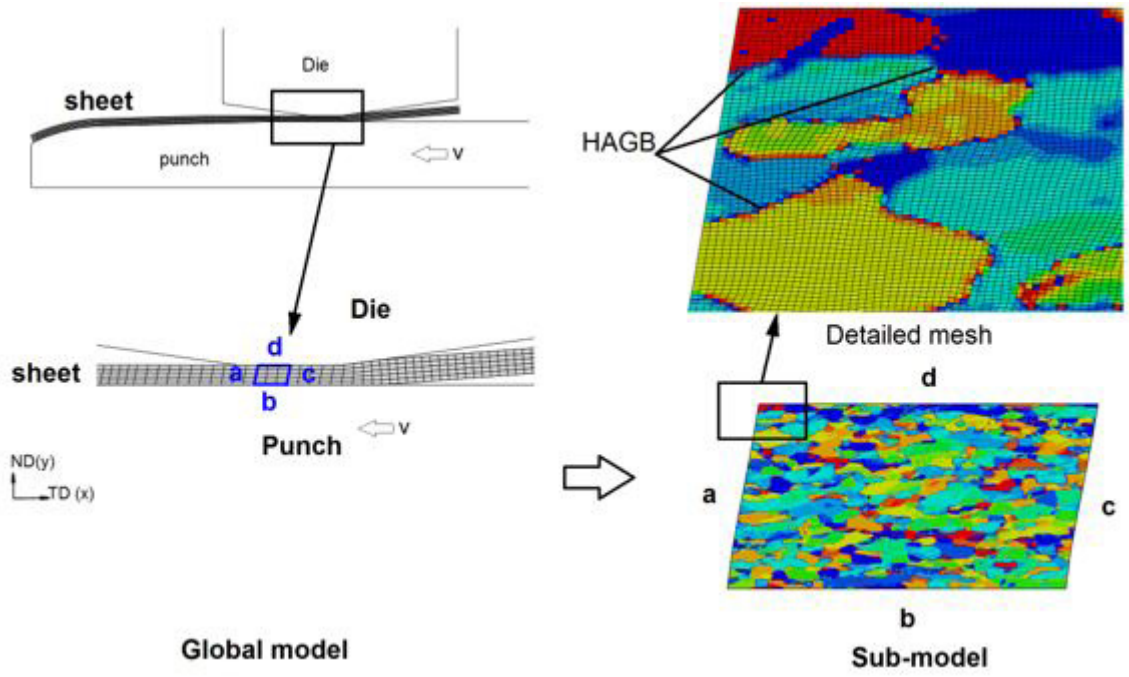

Figure 4: Schematic diagram of sub-modeling for ironing simulation, in the sub-model, the boundary conditions at edge a,b,c, d are driven by the displacement filed imported from the global model

In the sub-model, 99056 orientations represent grain structure in the selected region. Depending on orientation, each grain may have multiple orientations (elements). During ironing, shearing dominated nonuniform deformation within a grain generates a cell or subgrain structure within the grain. Shearing increase with the increase of ironing pass, which leads to the cell (sub-grain) size decreases and the misorientation between cells increases. Misorientation refers to the minimum angle θ_{min} among all crystallographically equivalent rotations that bring the lattices of adjacent grains into coincidence. Here, we use high-angle grain boundaries (HAGBs) to quantify grain misorientation developed within the original grain by grain subdivision. The HAGBs are those that have a misorientation greater than a critical value θ_c:

$\theta_{min} > \theta_c$ high-angle grain boundaries (HAGS)

$\theta_{min} < \theta_c$ low-angle grain boundaries

Based on initial grain misorientation, the grain boundary can be quantified by the number of misorientation (HAGBs) before and after ironing. The ratio of number of grain boundary of initial texture (N_{before}) and number of grain boundary of deformed texture (N_{after}), which represents grain refinement, is calculated by

$$\varphi = \frac{N_{before}}{N_{after}} \quad (5)$$

The constitutive behavior of crystal plasticity as described in Section 3 is applied to the sub-model while the isotrod pic plastic behavior of sheet (dash line in Figure 2) is applied to the global model through conventional von-Mises plasticity.

Results And Discussions

The selected area 0.981mm by 0.903 mm with EBSD measurement has been modeled by 328 elements in length and 302 elements in height with plane strain elements. The Euler angles of a total of 95066 orientations then are assigned to the model through field variables so that the model has the exact same texture map as the measured EBSD map. The key dimensions of the dies are listed in Table 1.

We first study 3-pass strip ironing process in the global model. After 3 ironing passes, the initial thickness of the sheet was reduced from 0.981 mm to 0.348 mm. It is also assumed that the coefficient of friction (COF) between the ironing dies and the sheet is 0.1. The deformation of the subsequent sub-model is driven by displacement boundary conditions from the global model for each individual ironing pass. Since our interest is to

study the deformation behaviors and texture evolution of ironed sheet, the results presented below are taken from the sub-model.

Figure 5 shows the distribution of 1st principles strain after each ironing pass in the sub-model. It is found that strong shear bands are formed in the first ironing pass, and are further intensified during the second and the third ironing passes. It is noted that both shear strain (sheared angle) and tensile strain (stretched length) increase with the increase of ironing pass and the decrease of thickness. The initial equalized grain structure has been sheared and stretched after 3 ironing passes. Some larger grains were broken down while some were severely stretched in the TD. The predicted texture evolution in terms of pole figure is presented in Figure 6. A typical shear texture is clearly observed after each ironing pass. Such increase in shearing is also supported by calculated R-values (not reported here) from the predicted texture. From the pole figures, the initial texture presents a strong shear texture. But, this initial texture intensity has been further spread out with the increase of the ironing pass, which implied that some new grain orientations and new grain boundaries were formed. This observation is consistent with the calculation from [13] and proves that shear strain plays a big role in forming the new grain boundaries.

Figure 7 shows the distribution of HAGBs on un-deformed and

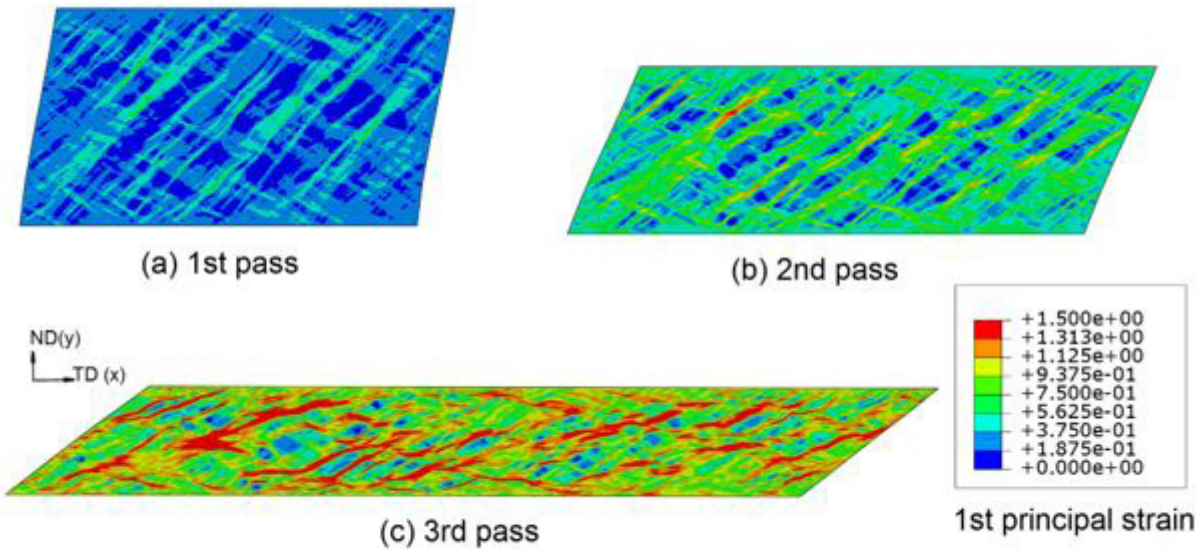

Figure 5: Distribution of the predicted 1st principal strain

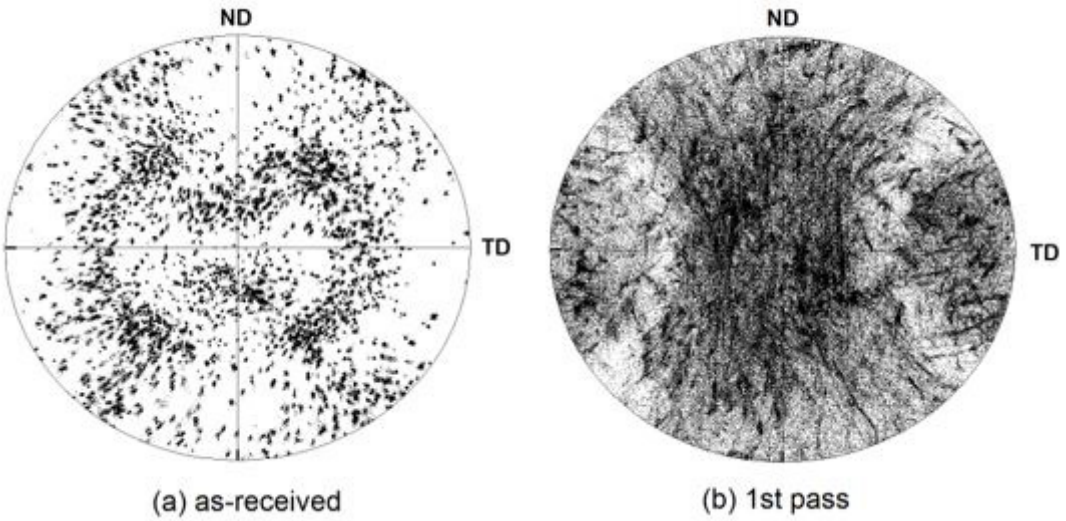

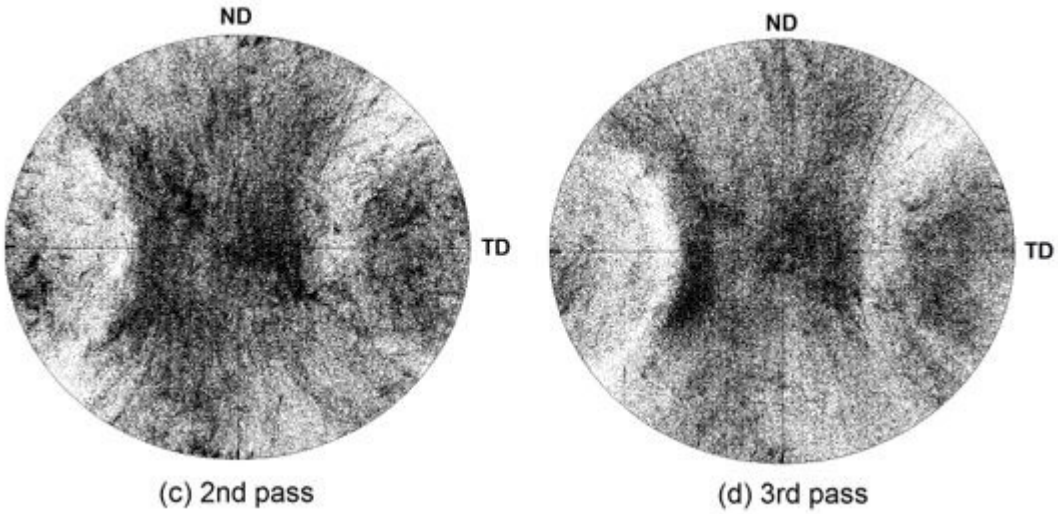

Figure 6: Predicted texture evolution after ironing ({1 1 1} pole figure plot)

deformed samples after 3 ironing passes, in which the critical misorienation is $\theta_c = 11°$. It is clear that the density of misorientation angle of selected area increases as ironing pass increases and shear strain increases, indicating the break-up of the initial grain structure and creation of new grain boundaries in ironing. Such trend is more obvious in the plot of misorientation angle on the un-deformed sample (squares on the left side in Figure 7) in comparison with initial misorientation angle plot. It is noted that the overall results and conclusions are not particularly dependent on the value of θ_c.

Using equation (5), the predicted grain refinement after ironing

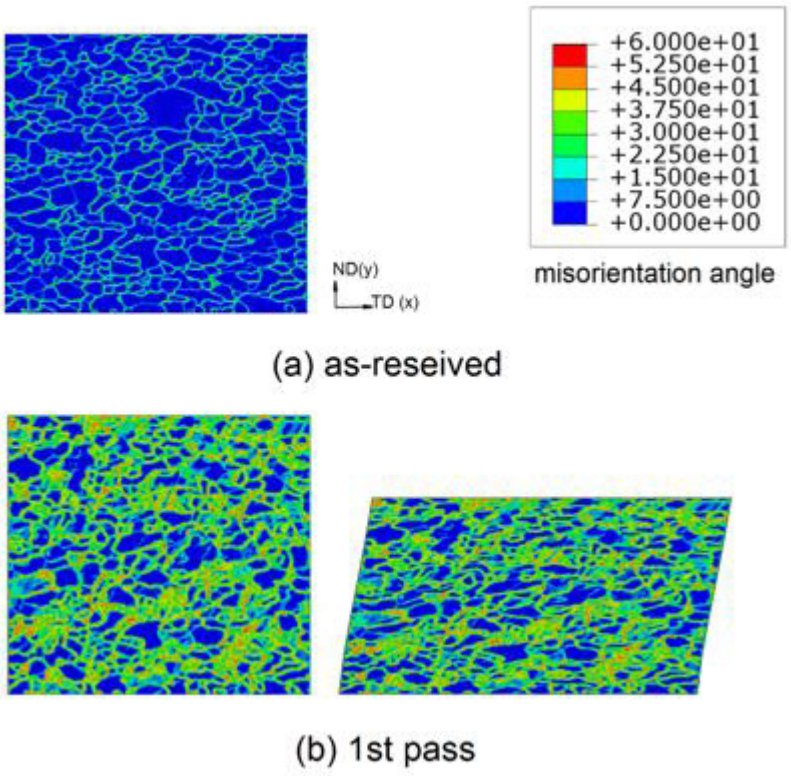

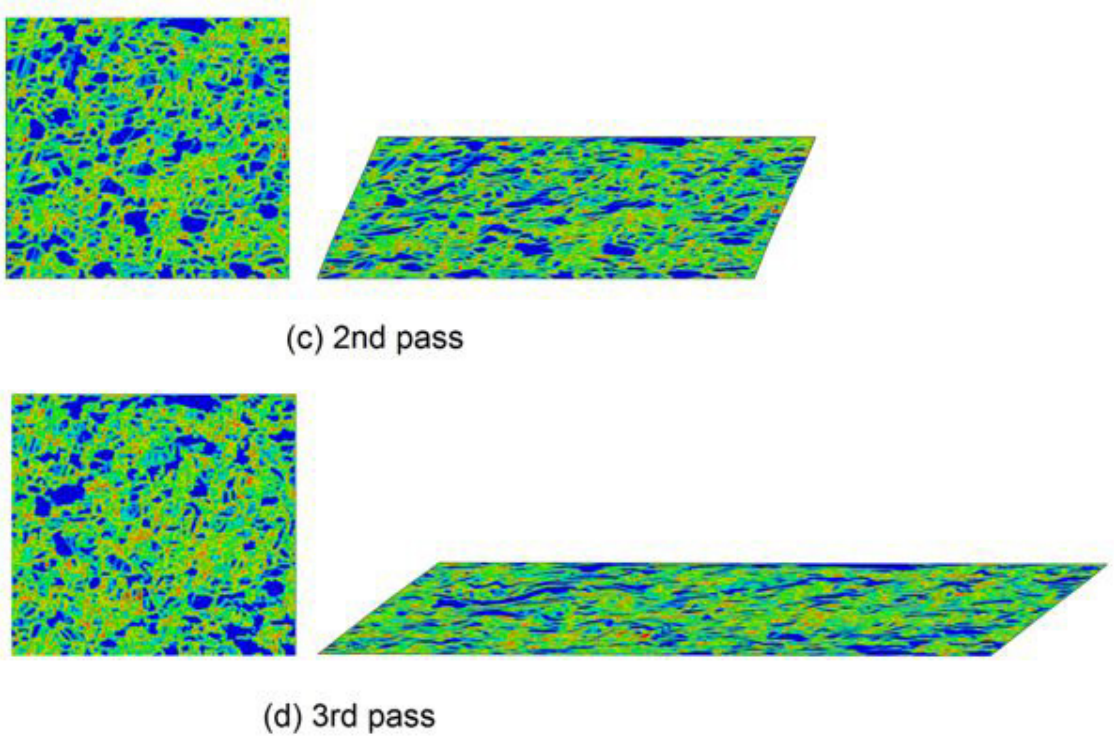

Figure 7: Predicted misorientation in ironing, left-side figure presents misorientation angle on non-deformed sample and right-side figure presents misorientation on deformed sample

in terms of thickness reduction is presented in Figure 8. It shows that grain size decreases monotonically with the increase of ironing passes. Among these three ironing passes, grain refinement is achieved mainly in the first ironing pass, in which grain boundary ratio φ is around 0.36 after the first ironing, followed by 0.30 and 0.28 after the second and third ironing, respectively. From Table 1, the first ironing takes only 23% thickness reduction of accumulated 62% reduction in ironing so the grain boundary ratio φ is not proportional to the sheet thickness reduction. The similar trends were observed in shear dominated deformation process such as ECAE ([14] and [13]). It may draw a conclusion that the first pass is the main contributor for grain refinement in shear dominated deformation process.

The effect of the step size of initial texture on grain re-

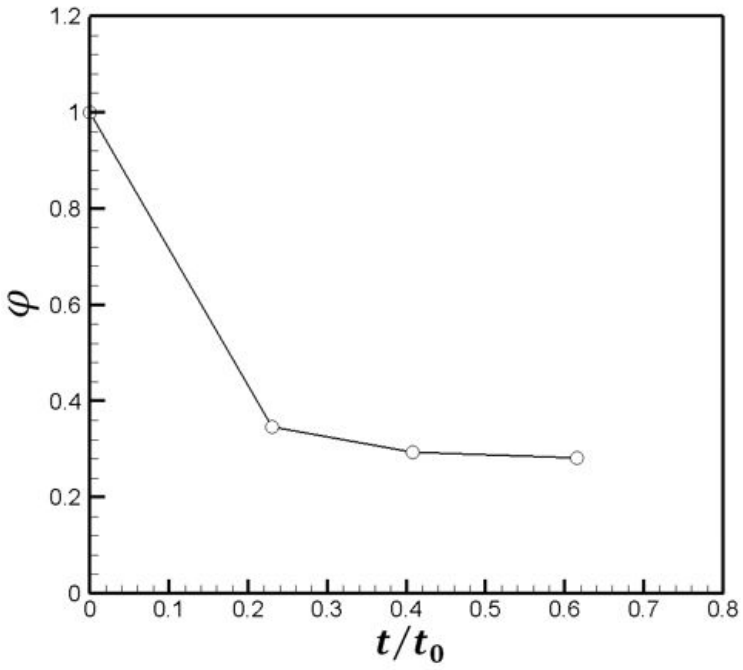

Figure 8: Predicted grain refinement against thickness reduction

finement

As reported in [13], texture evolution and grain refinement is influenced by the number of element per grain in the initial texture. Stated in section 4, the step size of the EBSD map is 3 m. To study the effect of step size of initial texture grain refinement, the step size was artificially doubled to 6 μm and halved to 1.5 μm from the measured size (3 μm). The step size 6 μm results in the element number being reduced by 75% per grain while the step size 1.5 μm will increase the element by 4 times per grain. The effect of step size of initial texture on grain refinement is plotted in Figure 9. It is found that step size 6 μm and step size 3 μm (measured) shows a noticeable difference in grain boundary ratio φ. While such difference is significantly reduced between the cases of step size 1.5 μm and step size 3 μm. After the third ironing pass, grain boundary ratio φ is very small or converged.

It is noted that the current approach of increase and

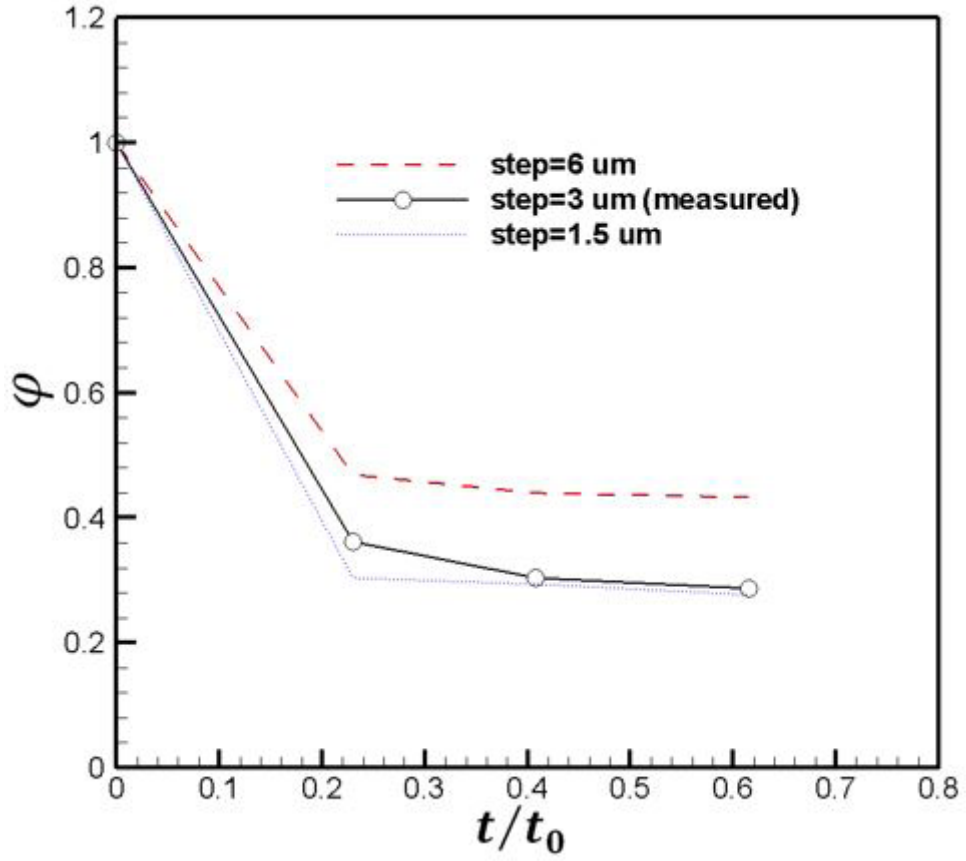

Figure 9: Effect of step size on grain refinement

decrease of the step size do not change grain orientations and its spatial distribution. Three cases will generate the same pole figures. The step size (or mesh density) of 6 μm seems to be too coarse to resolve grain-scale shear bands that are only fractions of a micron in thickness (see e.g. Humphreys et al. [18]). With the increase of mesh density (small step size), prominent features associated with grain fragmentation can be properly captured. The effect of element number per grain on grain refinement is also consistent with the calculation in [13].

Effect material strain rate sensitivity and work hardening on grain refinement

Material properties in crystal plasticity model plays important roles in sheet deformation, either under stretching or hydorforming (e.g. Wu et al. [19] and Shi et al. [20]). Figure 10 plots the effect of the strain rate sensitivity *m* on grain refinement as a function of thickness reduction. It shows that the increase of the rate sensitivity *m* (from 0.007 to 0.020) reduces grain refinement (increase of grain boundary ratio φ) slightly. Generally, the increase of the rate sensitivity tends to increase work hardening at a high strain level. However, the work hardening effect through increasing the rate sensitivity on grain refinements in ironing is limited.

The effect of critical resolved shear stress on grain refinement is

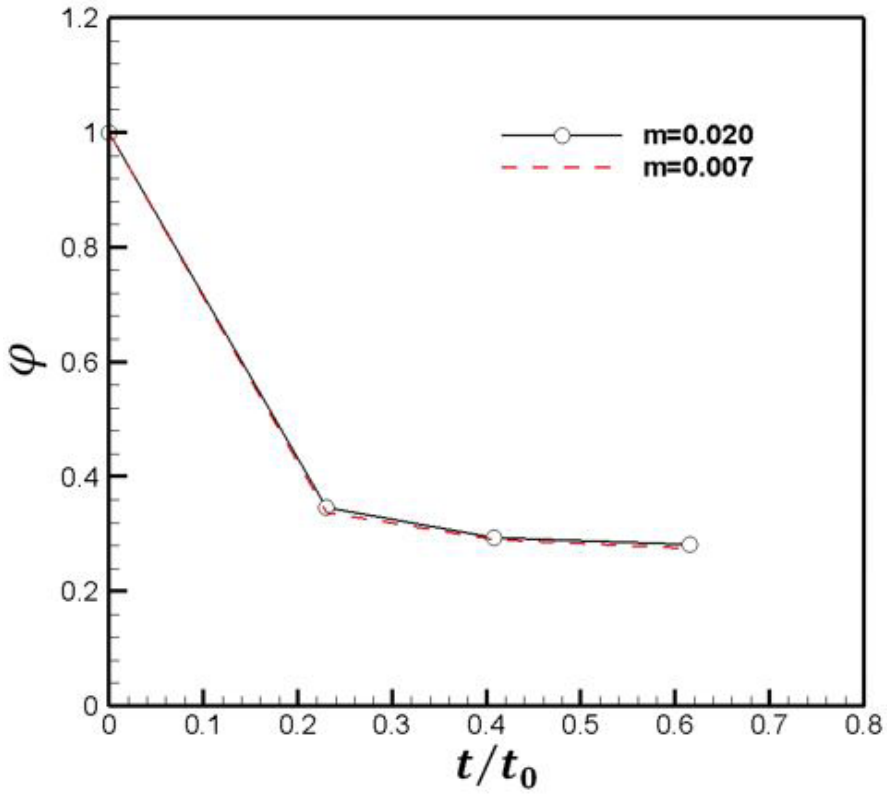

Figure 10: Effect of strain rate sensitivity on grain refinement

studied through increasing τ_s by a factor of 2 (from 112 MPa to 224 MPa) and results are plotted in Figure 11. It is observed that the texture refinement is reduced by an increase in work hardening. As stated in [20], in stretching deformation, increasing the work hardening rate will make relaxation processes more difficult, hence increase lattice resistance during shearing and stretching. However, the work hardening effect on grain refinements in the shearing dominated deformation is insignificant.

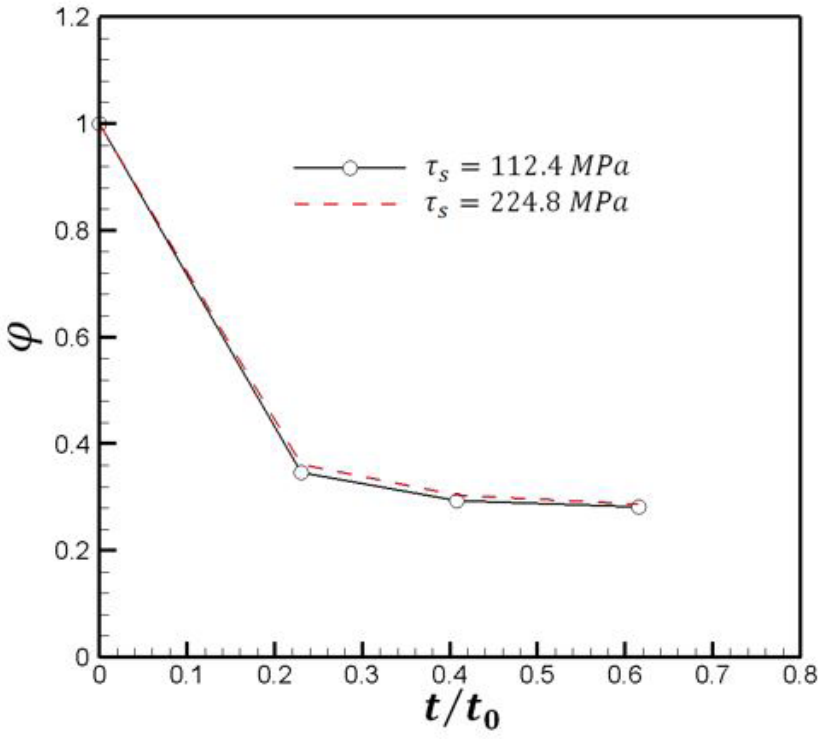

Figure 11: Effect of work hardening on grain refinement

Overall, grain refinement in ironing shows some sensitivity to material properties, such as strain hardening and material strain rate sensitivity. Lower strain rate sensitivity and/or lower hardening cause stronger grain-scale shear banding and thus result in more efficient grain refinement, but results show the effect of material properties on grain refinement during ironing is limited.

Effect friction in ironing on grain refinement

During the ironing process, friction between the sheet and dies is an important factor in assessing the ironability of the sheet. Too much friction will cause the extra loading force and may break the sheet in ironing. The optimized friction between die and sheet is normally in the range of 0.05 and 0.1. To study the effect of friction on grain refinement, we set the coefficient of friction (COF) between dies and the sheet to three values, 0.0, 0.1 and 0.2, respectively. Figure 12 compares grain refinement at these three COF values. Overall, high COF will result in high grain refinement. This is because that high friction between dies and the sheet tends to increase shearing which is plot in Figure 13. As studied by Wu [13] and Mishra [14], the amount of shear per pass has a significant effect on grain refinement in equal-channel angular pressing (ECAP). The friction-induced shear strain contributes to the grain refinement in a similar way in the ironing process. Probably, shear strain in ironing does not change as drastically as those in ECAP, which results in limited percentage of change in grain refinement.

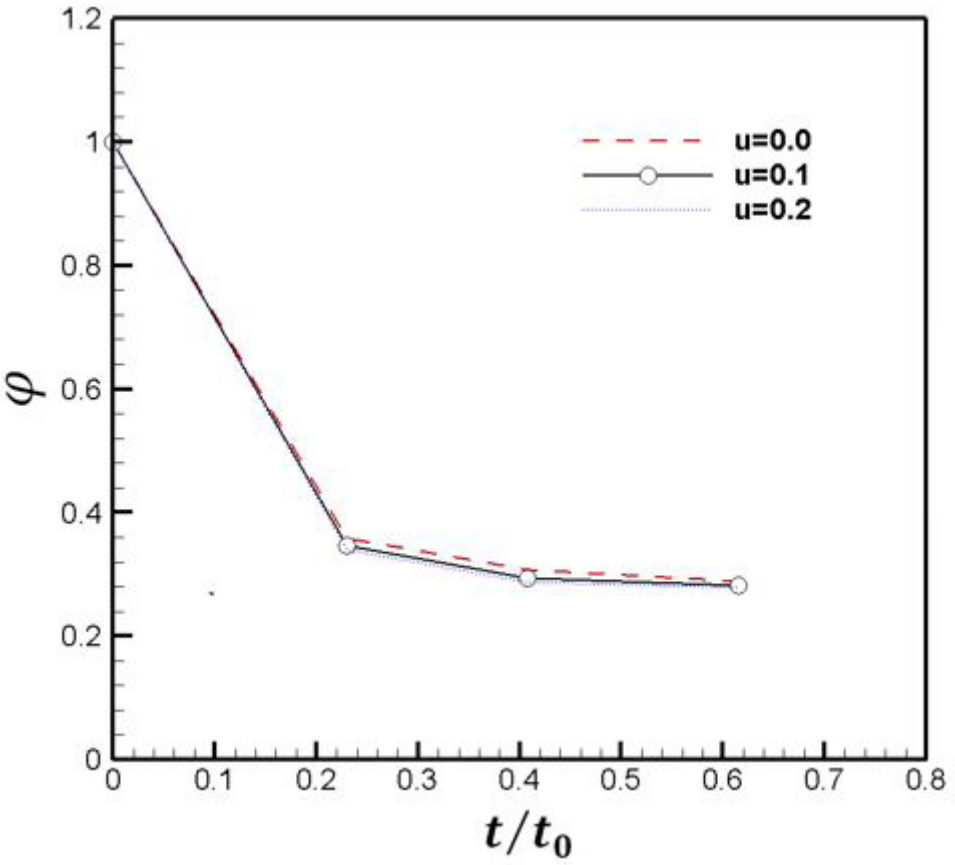

Figure 12: Effect of coefficient of friction (COF) on grain refinement

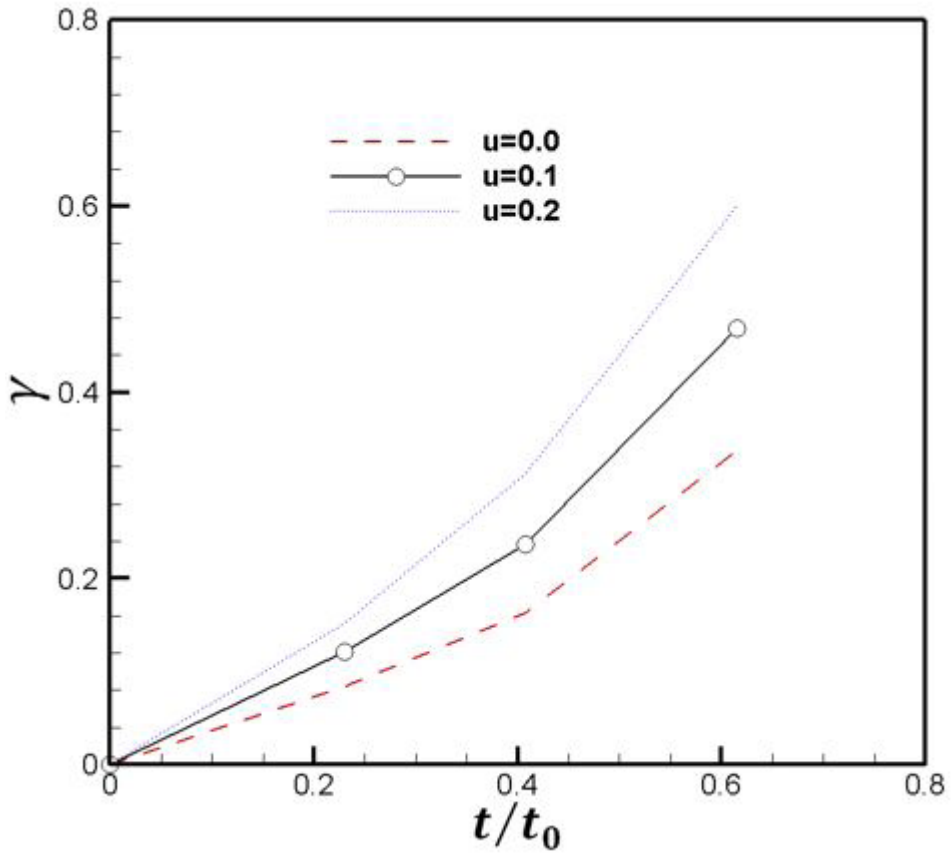

Figure 13: Effect of coefficient of friction (COF) on shear strain γ

Effect ironing thickness reduction and ironing passes on grain refinement

The main purpose the ironing operation is to reduce the sheet thickness and increase the sheet length in a repetitive ironing operation. To study the ironing reduction and ironing pass on grain structure evolution and grain refinement, we increased the ironing passes from 3 to 4 and 5, but keep the total thickness reduction unchanged (from 0.981 mm to 0.348 mm). For a 3-pass or a 4-pass ironing, the absolute thickness reduction in each pass (reduction increment) is kept the same as well. The ironing reduction set up is listed Table 1.

Table 1: Die Dimensions

	Accumulated reduction (%)			Die key dimensions
	3-pass	4-pass	5-pass	
Die 1	23	15	12	Entry angle (α): 8 degrees Exit angle (β): 8 degrees Landing length (s): 3.6 mm
Die 2	41	31	25	
Die 3	62	46	37	
Die 4	-	62	49	
Die 5	-	-	62	

The grain refinement (grain boundary ratio φ) in terms of thickness reduction is plotted in Figure 14. It is found that 3-pass, 4-pass and 5-pass ironings generate the same grain refinement after the final ironing pass, even though each individual pass may result in different values of grain boundary ratio φ. By examining the shear strain level, it reveals that the total accumulate shear strains are almost identical for these three ironing routes even though each ironing route has its different thickness reduction percentage as listed in Table 1. It is worth to mention that except the ironing pass difference, the rest of the parameters such as material, friction are identical. This study shows that texture grain refinement is independent of the ironing pass for a given ironing reduction. It also proves that shear strain is one of important factor which influences the texture evolution and new grain boundary formation in ironing process.

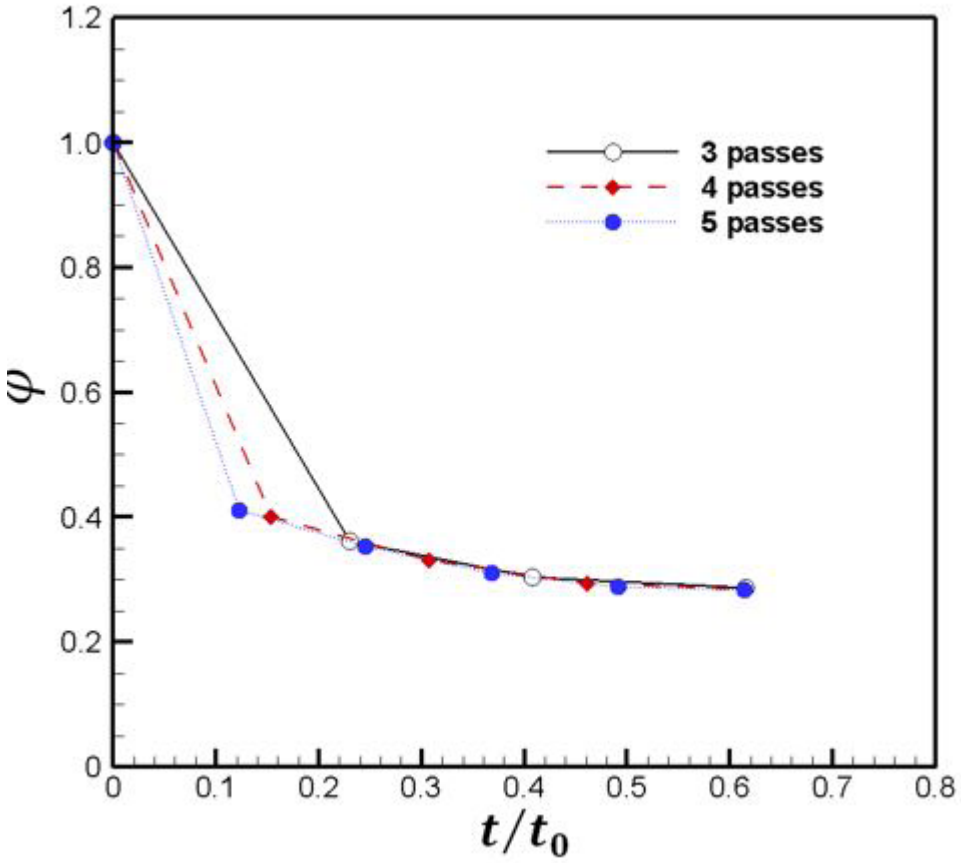

Figure 14: Effect of reduction and ironing pass on grain refinement

Summary

A plane strain crystal plasticity finite element model is developed to simulate sheet strip ironing operation. The measured EBSD data for the sheet is mapped to the selected sheet area and then directly incorporated into the crystal plasticity finite element model. The ironing simulations examined the distributions of plastic strain and high angle grain boundaries as well as texture evolution. The main findings are as follows

1. Grain refinement is mainly established in the first ironing pass
2. The friction-induced shear strain in each ironing pass influences on sheet texture evolution even though such texture evolution may be path-independent as long as the total thickness reduction keeps the same.
3. A very small step (fine mesh) is necessary to resolve grain-scale shear bands.
4. The material properties such as rate sensitivity and work hardening also play a limited role in texture evolution during ironing. Lower strain rate sensitivity and/or lower hardening cause stronger grain-scale shear banding and thus result in more efficient grain refinement.

Acknowledgements

This work is supported by the Natural Sciences and Engineering Research Council of Canada (NSERC).

References:

1. G. E. Dieter (1988) "Mechanical Metallurgy". Singapore: McGraw Hill.

2. M. Schünemann, M. A.Ahmetoglu and T. Altan, (1996) "Prediction of process conditions in drawing and ironing of cans", Journal of Materials Processing Technology, 59:1-9.

3. F. Heymis, J. D. Embury, R. Sowerby and U. F. Kocks, (1995) "Deformation and texture evolution of a 3004 aluminium alloy during ironing", Textures and Microstructures, 25:1-15.

4. Y. Abe, T. Fujita, K. Mori, K. Osakada, T. Shiba and W. Daodon, (2014) "Improvement of formability in ironing of stainless steel drawn cups using low friction cermet dies", Procedia Engineering, 81:1896-01.

5. S. Singh, V. Kumar, P. Reddy and A. Gupta, (2014) "Finite element simulation of ironing process under warm conditions", Journal of Materials Research and Technology, 3:71-78.

6. A. Anggono and W. Siswanto, (2014) "Simulation of Ironing Process for Earring Reduction In Sheet Metal Forming", Applied Mechanics and Materials, 46:91-95.

7. H. Jin and D.J. Lloyd, (2005) "The reduction of planar anisotropy by texture modification through asymmetric rolling and annealing in AA5754", Materials Science and Engineering: A, 399:358-67

8. H. Jin and D.J. Lloyd, (2010) "The different effects of asymmetric rolling and surface friction on formation of shear texture in aluminium alloy AA5754", Materials Science and Technology, 26:754-60.

9. S. Wronski and B. Bacroix, (2014) "Microstructure evolution and grain refinement in asymmetrically rolled aluminium", Acta Materialia 76:404-12.

10. S. Tamimi, J. P. Correia, A. Lopes, S. Ahzi, F. Barlat and J.Gracio, (2014) "Asymmetric rolling of thin AA-5182 sheets: Modelling and experiments",Materials Science & Engineering: A, 603:150-59.

11. S.M. Sivakumar and M. Ortiz, (2004) "Microstructure evolution in the equal channel angular extrusion process", Computer Methods in Applied Mechanics and Engineering, 193:5177-94.

12. A. Mishra, V. Richard, F. Gregori, R.J. Asaro and MA Meyers, (2005) "Microstructural evolution in copper processed by severe plastic deformation", Materials Science and Engineering: 410:290-98.

13. P.D. Wu, Y. Huang, and D.J. Lloyd, (2006) "Studying grain fragmentation in ECAE by simulating simple shear", Scripta Materialia, 54:2107-12.

14. M.H. Shaeri, M. Shaeri, T.Salehi, S.H. Seyyedein and F.Djavanroodi, (2015) "Microstructure and texture evolution of Al-7075 alloy processed by equal channel angular pressing", Transactions of Nonferrous Metals Society of China, 25:1367-75.

15. R.J. Asaro and A. Needleman, (1985) "Texture development and strain hardening in rate dependent polycrystals", Acta Materialia, 33:923-53.

16. P.D. Wu, K.W. Neale and E. Van der Giessen, (1996) "Simulation of the behavior of FCC polycrystals during reversed torsion", International Journal of Plasticity, 12:1199-19.

17. ABAQUS User Manual, 2013, Version 6.13.

18. F.J. Humphreys, P.B. Prangnell, J. R. Bowen, A. Gholinia and C Harris, (1999) "Developing stable fine–grain microstructures by large strain deformation", Philosophical Transactions of the Royal Society of London. Series A: Mathematical, Physical and Engineering Sciences, 357:1663-81.

19. P.D. Wu, D. J. Lloyd, M. Jain, K. W. Neale., Y. Huang, (2007) "Effects of spatial grain orientation distribution and initial surface topography on sheet metal necking", International Journal of Plasticity, 23:1084-04.

20. Y. Shi , P.D. Wu, D.J. Lloyd, J.D. Embury, (2010) "Crystal plasticity based analysis of localized necking in aluminum tube under internal pressure", European Journal of Mechanics A/Solids, 29:475-83.